Normal-state correlated electronic structure of the tetragonal $TlNi_2Se_2$ superconductor

L. Craco[1,2] and S. Leoni[3]

[1]Institute of Physics, Federal University of Mato Grosso, 78060-900 Cuiabá, Mato Grosso, Brazil
[2]Leibniz Institute for Solid State and Materials Research Dresden, D-01069 Dresden, Germany
[3]School of Chemistry, Cardiff University, Cardiff CF10 3AT, United Kingdom

(Received 13 March 2023; revised 19 May 2023; accepted 14 July 2023; published 27 July 2023)

On the basis of density functional plus dynamical mean-field theory calculations we explore the electronic structure of the $TlNi_2Se_2$ superconductor, showing how the normal-state spectra are reshaped by dynamical many-particle interactions. Upon electron-doping the $3d^8$ Fermi liquid metal, hidden orbital selectivity with coexisting Mott localized, pseudogapped, and narrow Kondo-quasiparticle electronic excitations is predicted for $TlNi_2Se_2$. By specifically focusing on the energy spectrum that is relevant to the mixed-valence heavy-electron normal state of unconventional superconductors, our findings have the potential to enhance our microscopic understanding of the intricate interplay between many-particle physics and electron band filling, paving the way for further advancements.

DOI: 10.1103/PhysRevB.108.045140

I. INTRODUCTION

Since its discovery in 2008 [1], multiorbital (MO) unconventional superconductivity in tetragonal layered materials has become a prominent area of research in condensed matter and materials science. Significant progress has been made in understanding the origins and interdependence of various phases in this category of correlated electron systems. The ongoing discussions surrounding the transition from the normal state to unconventional superconductivity have had a significant impact on the debate about correlated electronic structure reconstruction and potential phase instabilities. A key point of contention has been determining whether superconductivity arises from a pairing instability of a Fermi liquid (FL) metal or as a non-Fermi liquid near an orbital-selective Mott metal-insulator transition [2].

One effective approach to answering this fundamental question is to conduct a systematic investigation of different members of the family of MO tetragonal transition-metal superconductors. It has accordingly become increasingly evident that these materials exhibit bad-metal behavior in their normal, paramagnetic state, where the electrical resistivity deviates considerably from the canonical FL T^2 behavior as $T \rightarrow 0$ [3]. In strongly correlated electron systems, $\rho(T)$ typically follows a power-law behavior with $1 < n < 2$ in the bad-metal state, reflecting the development of a highly renormalized lattice coherence scale resulting from the growing relevance of dynamic MO electronic correlations as temperature decreases.

In this context, the discovery of multiband [4] and multigap nodeless [5] superconductivity, along with $\rho(T) = \rho_0 + AT^2$ behavior observed from 25 K down to temperatures near $T_c = 3.7$ K in the 122-type Ni chalcogenide $TlNi_2Se_2$ (see Fig. 1), is noteworthy. This finding adds another member to the tetragonal superconducting family, where superconductivity emerges in the parent compound under ambient pressure. Similar to the LiFeAs superconductor and in contrast to most Fe-based superconductors [6], $TlNi_2Se_2$ has no magnetic or structural phase instabilities. Compared with Fe-based superconductors, Ni-based systems have lower superconducting critical temperatures, which are usually below 5.0 K even upon doping [7]. To date, there is no evidence for ordered or even fluctuating magnetism associated with Ni in the normal state. Although under debate [8–10], for KNi_2X_2 ($X =$ Se, S) [11,12] and $TlNi_2Se_2$ [4], the weakly correlated electronic state that gives rise to pseudogap formation in optics [13] and unconventional superconductivity [10] seems to involve heavy-electron [4,11] behavior below a FL coherent temperature that is driven by mixed valence.

In contrast to KFe_2Se_2 [14], the Ni-based 122-type compounds are homogeneous without Ni vacancy or phase separation [4,11]. It has been argued that the effective valence of 122-type Ni compounds is 1.5+. The mixed valency of $Ni^{1.5+}$ is believed to be responsible for the heavy-electron effective mass $m^* = (6\text{–}20)m_e$ [4,11] inferred from extant electronic specific heat studies. This view is supported by angle-resolved photoemission spectroscopy studies, suggesting that neither $TlNi_2Se_2$ [9] nor KNi_2Se_2 [8] is a strongly correlated material and that the camelback-shaped band at the Z point gives rise to a Van Hove singularity near the Fermi energy E_F in $TlNi_2Se_2$ [9], providing a one-band explanation for the heavy-electron behavior in a system governed by weak Coulomb correlations [8]. However, the consequences of orbital selectivity and proximity to electronic localization in tetragonal 122-type Ni superconductors have not received enough attention, in spite of hidden heavy electrons with considerably large effective masses [4,11,12,15].

LiFeAs is considered a weakly correlated Fermi liquid metal with an on-site Coulomb interaction U of around 2.5 eV [16]. In contrast, our findings indicate that the $3d^8$ (Ni^{2+}) valent state of $TlNi_2Se_2$ is considerably more correlated than that of LiFeAs, displaying a first-order metal-insulator transition at a critical U value ranging between 2.4 and 2.5 eV. This insight helps to further the ongoing discussion [17]

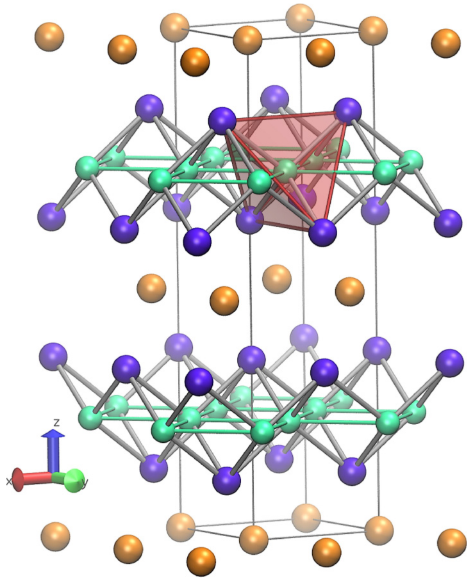

FIG. 1. Crystal structure of the tetragonal $TlNi_2Se_2$ superconductor (Ni, green; Tl, orange; Se, violet). The tetragonal coordination of Ni by Se is represented as a red tetrahedron. The tetragonal unit cell is drawn in gray.

about the connection between the level of MO electronic correlations and the proximity to Mottness unconventional superconductors.

In this paper, we investigate the role of dynamical MO electronic correlations in the electronic structure reconstruction in the Ni-3d shell of both self-hole-doped (Ni^{2+}, see our discussion below) and mixed-valence ($Ni^{1.5+}$) $TlNi_2Se_2$. As shown in our earlier studies on MO Fe-based superconductors [18–20], all five 3d bands need to be considered in order to satisfactorily resolve the correlated electronic state composed of heavy particles in stoichiometric ($d^{8.5}$) $TlNi_2Se_2$. In MO systems near selective Mott localization, changes in many-particle interactions and electron band filling can lead to interesting physical effects driven by electronic correlations. These tunable degrees of freedom can create an exotic regime where the chemical potential is found in an energy region with almost zero density of states (DOS), resulting in a coexistence of metallic, insulating, and pseudogapped electronic states. To study these phenomena, we employ the density functional plus dynamical mean-field theory (DFT+DMFT) framework and examine the correlated normal state of the $TlNi_2Se_2$ superconductor. Additionally, we discuss the influence of FL metallicity and selective Mottness and provide specific predictions that can be tested in future studies.

II. RESULTS AND DISCUSSION

MO physics is inherently complex due to orbital and spin degrees of freedom. These coupled correlations have been hampering fully realistic theoretical studies. In recent years, however, the DFT+DMFT approximation [21] has established itself as a reference computational framework that allows for a systematic approach to the treatment of MO electronic correlations in real crystals. Here, we used DFT to calculate Bloch electronic states in the Perdew-Burke-Ernzerhof (PBE) approximation using Vanderbilt ultrasoft standard solid state pseudopotentials (SSSP) [22]. The plane-wave expansion of valence electron wave functions and charge density used kinetic energy cutoffs of 75 and 650 Ry, respectively. Calculations were performed using the PW.X code (v6.7) of the QUANTUM ESPRESSO (QE) package. The crystal structure data obtained from experiments (see Fig. 1) were used as input [23]. Self-consistent-field (SCF) calculations were run on a k grid of $8 \times 8 \times 8$ data points. A tight-binding band structure model was obtained from interpolating maximally localized Wannier functions (MLWFs), calculated with the WANNIER90 package (v3.1) [24]. As the initial guess for the Wannier functions, 3d orbitals were used for Ni (ten MLWFs in total). Iterative spread minimization provided real-valued, maximally localized Wannier functions using a 1.0×10^{-12} Ω convergence tolerance. Forty-seven Bloch states were considered (outer energy window maximum 18.0 eV). An inner, frozen energy window in the range 8.2–11.75 eV was used to disentangle ten states for Wannierization. The choice of those energy ranges guarantees Ni localized, atomic-like, orthogonal Wannier functions, with the correct site symmetry and intersite symmetry equivalence (Fig. 2). The space group symmetry compliance of the Wannier Hamiltonian after spread minimization was checked with WANNIERTOOLS [25]. The quality of the Wannier fit is shown in Fig. 3. The resulting orbital-resolved DFT DOS is displayed in Fig. 4. Consistent with earlier band structure calculations for tetragonal Ni-based superconductors [26], the line shape of the bare DOS is strongly orbital dependent, showing MO all-electron metallicity within the Ni-d^8 oxidation state in contrast to the KFe_2Se_2 superconductor [19], due to there being more 3d electrons in $TlNi_2Se_2$ than in KFe_2Se_2.

Similar to Fe-based superconductors [18,19] as well as to infinite-layer Ni superconductors [27], the one-electron part of the Ni-3d model Hamiltonian [28–30] relevant to the normal paramagnetic state of $TlNi_2Se_2$ is $H_0 = \sum_{\mathbf{k},a,\sigma} \epsilon_a(\mathbf{k}) c^\dagger_{\mathbf{k},a,\sigma} c_{\mathbf{k},a,\sigma} + \sum_{i,a,\sigma} (\epsilon^{(0)}_{a,\sigma} - \mu) n_{i,a,\sigma}$, where $a = x^2-y^2, 3z^2-r^2, xz, yz, xy$ denotes the 3d orbitals of $TlNi_2Se_2$. Here, $\epsilon_a(\mathbf{k})$ is the corresponding band dispersion, which encodes details of the one-electron (DFT) band structure, and $\epsilon^{(0)}_{a,\sigma} \equiv \epsilon_a - U(n_{a,\bar{\sigma}} - \frac{1}{2}) + \frac{J_H}{2}(n_{a,\sigma} - 1)$. ϵ_{ia} is the on-site energy of a given 3d orbital, and the other terms are subtracted therefrom to avoid double-counting of interactions already treated on average by DFT [31]; J_H is the Hund's coupling. Finally, μ is the chemical potential of the system. These five Ni-3d orbitals are the relevant one-particle inputs for MO-DMFT, which generates a renormalized electronic state as shown below. Moreover, consistent with our earlier studies, the correlated many-body Hamiltonian considered for $TlNi_2Se_2$ reads $H_{\rm int} = U \sum_{i,a} n_{i,a,\uparrow} n_{i,a,\downarrow} + U' \sum_{i,a\neq b} n_{i,a} n_{i,b} - J_H \sum_{i,a\neq b} \mathbf{S}_{i,a} \cdot \mathbf{S}_{i,b}$. Here, $U' = U - 2J_H$ is the interorbital Coulomb interaction term. Given the complexity of the MO problem, with diagonal and off-diagonal lattice Green's functions and self-energies [32], here we work in the basis that diagonalizes the one-particle density matrix. In this basis, interorbital one-electron overlap is zero, and so in the paramagnetic phase we have $G_{a,b,\sigma}(\omega) = \delta_{a,b} G_{a,\sigma}(\omega)$ [31]. In this regime, electrons among different orbitals interact only via the interorbital Coulomb interaction and the

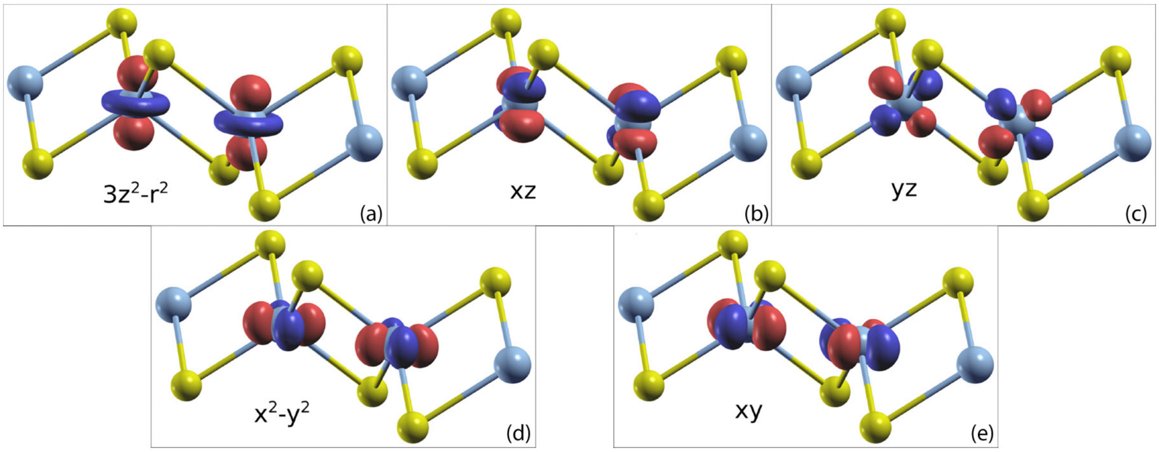

FIG. 2. Wannier functions for the two symmetry-equivalent Ni sites in $TlNi_2Se_2$, in the Wannier projections (a) $3z^2 - r^2$, (b) xz, (c) yz, (d) $x^2 - y^2$, and (e) xy. Isosurfaces are interpolated at ± 3.53 (red and blue lobes). Ni, gray; Se, yellow. The distorted tetrahedral Se coordination around Ni is shown. Wannier functions display (D_{2d}) close-to-atomic character.

Hund's coupling. We evaluate the retarded Green's functions [$G_a(\mathbf{k}, \omega) = \frac{1}{\omega - \Sigma_a(\omega) - \epsilon_a(\mathbf{k})}$, with $\Sigma_a(\omega)$ being the Ni-3d self-energy of orbital a] of the many-particle problem of $TlNi_2Se_2$ using the multiorbital iterated perturbation theory (MO-IPT) as impurity solver within DMFT. This interpolative *ansatz* is known to account for the correct low- and high-energy behavior of the one-particle spectral function and self-energies of MO Hubbard-like models in the infinite-dimension limit (DMFT). It ensures the Mott-Hubbard metal-insulator transition from a correlated metal to a Mott insulator as a function of the Coulomb interaction U. The MO-IPT scheme is computationally very efficient, with real-frequency output at zero temperature, enabling the study of electronic structure reconstruction of real materials with different phase instabilities. The full set of equations for the MO case can be found, for example, in Ref. [33]; therefore we do not repeat the equations here. This real-frequency perturbative scheme has a proven record of good semiquantitative agreement with experiment for a range of correlated materials, and it gives results in qualitative accord with numerically exact continuous-time quantum Monte Carlo (CT-QMC) calculations for the tetragonal FeSe superconductor [34], in spite of the fact that fully charged self-consistent DFT+DMFT calculations are presently unreachable within our scheme.

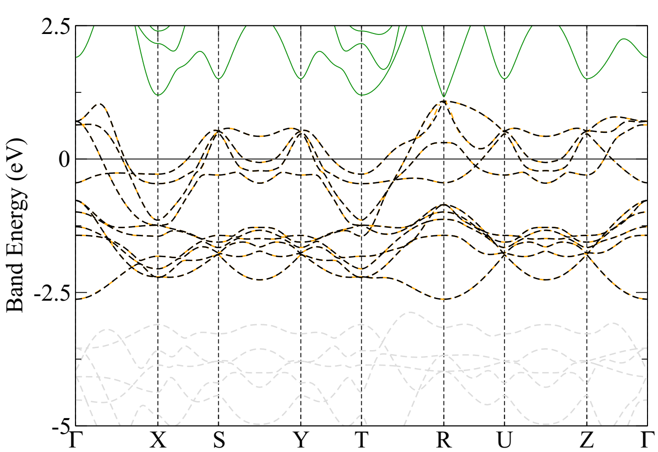

FIG. 3. Band structure of $TlNi_2Se_2$, calculated along Γ-X-S-Y-T-R-U-Z-Γ. The Wannier band structure model (orange dashed lines) is displayed for the ten 3d bands (black dashed lines) around the Fermi level. Further occupied (gray dashed lines) and empty bands (green) are shown.

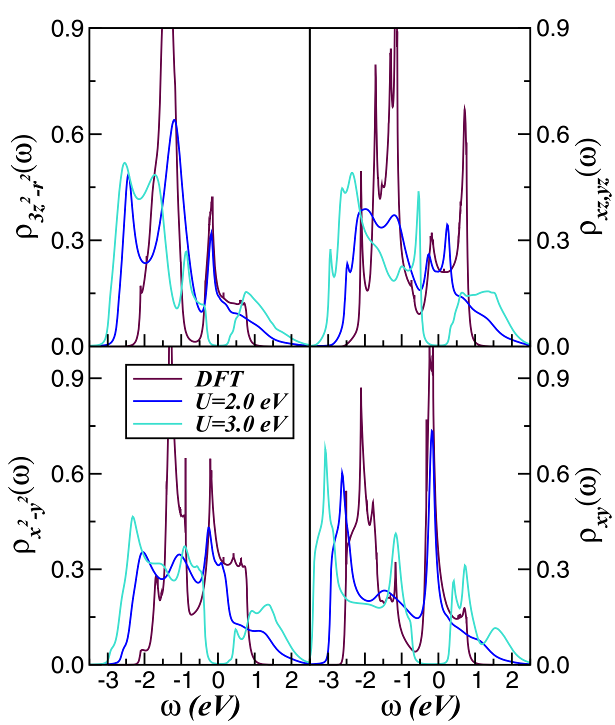

FIG. 4. DFT and DFT+DMFT orbital-resolved density of states (DOS) of the tetragonal $TlNi_2Se_2$ superconductor, showing spectral weight redistribution over large energy scales with increasing on-site Coulomb interaction U within the Ni-3d^8 electronic configuration. While all orbitals are metallic at $U = 2.0$ eV, Mott localization is obtained for $U = 3.0$ eV. Here, all DFT+DMFT(MO-IPT) spectral functions are computed at zero temperature.

The IPT approach is an interpolative *ansatz* that connects the two exactly soluble limits of the one-band Hubbard model [35], namely, the uncorrelated ($U = 0$) and the atomic [$\varepsilon(\mathbf{k}) = 0$] limits. It accounts for the correct low- and high-energy behavior of the one-particle spectra, and the metallic FL behavior in the large-D limit (DMFT) [36]. It ensures the Mott-Hubbard metal-insulator transition from a correlated FL metal to a Mott-Hubbard insulator as a function of the Coulomb interaction U. As shown below, the DFT+DMFT(MO-IPT) solution for $TlNi_2Se_2$ introduces nontrivial effects stemming from the dynamical nature of strong electronic correlations. These processes lead to transfer of spectral weight across large energy scales in response to changes in the on-site Coulomb repulsion, a characteristic lying at the heart of the anomalous responses of correlated electron systems. We recall that a similar perturbative scheme to that used here for the MO Hamiltonian of $TlNi_2Se_2$ has been proposed in Ref. [37], where electron correlation effects in local-orbital electronic structure calculations were applied to Si bulk crystals and H_2O molecules. It is also worth noting that direct comparisons between MO-IPT results with numerically exact methods, such as the CT-QMC, have been performed in recent years [38], showing good qualitative agreement between the two impurity solvers. Hence, in view of this and our previous studies on correlated electron systems showing good theory-experiment agreement [31,34], we are confident in using MO-IPT to explore the normal-state electronic structure reconstruction of the $TlNi_2Se_2$ superconductor.

Since the effect of electronic correlations in the excitation spectrum of $TlNi_2Se_2$ and analogs is not fully understood yet, in Fig. 4 we compare the DFT orbital-resolved DOS with the corresponding renormalized spectral functions to highlight the electronic structure evolution which emerges with increasing the on-site Coulomb interaction U and fixed $J_H = 0.7$ eV [29]. To obtain the total orbital occupations, the DFT+DMFT equations are constrained by the sum rule $n_{\rm total} = \int_{-\infty}^{\mu} \rho(\omega)_{\rm total} d\omega \equiv n$ [39]. The chemical potential μ is then determined self-consistently within the DFT+DMFT loop at each stage using $\rho_{\rm total}(\omega) = \sum_a \rho_a(\omega)$ computed in each iteration. As seen in Fig. 4, upon consideration of MO dynamical correlations, the sharp and well-defined singular features of the bare electronic structure are smeared on all Ni-3d orbitals. Many-particle MO self-energy corrections induced using an on-site Coulomb interaction $U = 2.0$ eV lead to the emergence of lower and upper Hubbard bands (LHB and UHB, respectively) in the valence and conduction bands at energies close to ± 1.0 eV on all orbitals for the $3d^8$ electronic configuration of self-hole-doped $TlNi_2Se_2$. While some sharp features remain visible in the xz, yz, and xy spectral functions at high binding energies, the overall spectra are considerably broadened compared with the bare spectral functions. Interestingly, at $U = 2.0$ eV all orbitals reveal emergent FL quasiparticles [36] at low energies. However, at $U = 3.0$ eV all-electron localization is induced in tetragonal $TlNi_2Se_2$, which is characterized by a pronounced Mott-Hubbard gap near $E_F = \omega = 0$. A similar insulating state could possibly be seen in future studies on strained $TlNi_2Se_2$ crystals, due to an enhanced U/W ratio via strain-induced one-particle band narrowing [40]. Taken together, our

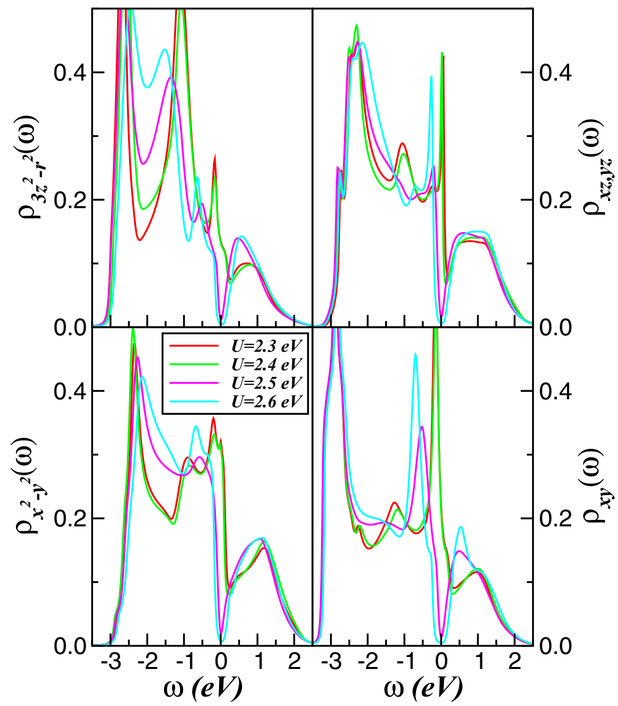

FIG. 5. Orbital-resolved spectral functions of self-hole-doped $TlNi_2Se_2$, showing their evolution with increasing U for fixed $J_H = 0.7$ eV. A particular feature to be seen is the abrupt Mott metal-insulator transition at a critical U between 2.4 and 2.5 eV on all orbitals within the Ni-$3d^8$ state.

results in Fig. 4 reveal the coexistence of Kondo quasiparticles and incoherent electronic excitations on all Ni-3d orbitals of $3d^8TlNi_2Se_2$. Future polarized x-ray emission and absorption spectroscopy studies are called for to confirm our prediction for the orbital-resolved electronic spectrum of the unstrained $TlNi_2Se_2$ superconductor.

We shall notice here that while incoherent, bad metals are characterized by pseudogapped electronic excitations near E_F, coherent FL metals show, on the other hand, narrow Kondo-quasiparticle resonances. The Kondo quasiparticle, also referred to as the Abrikosov-Suhl resonance [36], is a key feature of the FL metal, in which the spin-flip scattering process leads to the formation of a many-body bound state known as the Kondo resonance. The Kondo resonance is a quasiparticle excitation that appears as a sharp peak in the one-particle spectral function at low temperatures. The fingerprint of the Kondo quasiparticle can be observed in the low-energy spectral function, which in systems away from half filling displays a characteristic asymmetry in the peak shape. The observation of the Kondo quasiparticle in the one-particle spectral function provides a direct probe of Kondo-like (multiorbital or not) physics, and it has been used to study a wide range of coherent FL metals and heavy-fermion materials, among other quantum many-particle systems.

For a more detailed analysis of dynamical MO correlation effects, in Fig. 5 we display the abrupt changes in the spectral functions across the first-order metal-to-insulator transition, which could possibly be seen in future studies on strained $TlNi_2Se_2$. As seen in this figure, MO electronic correlations

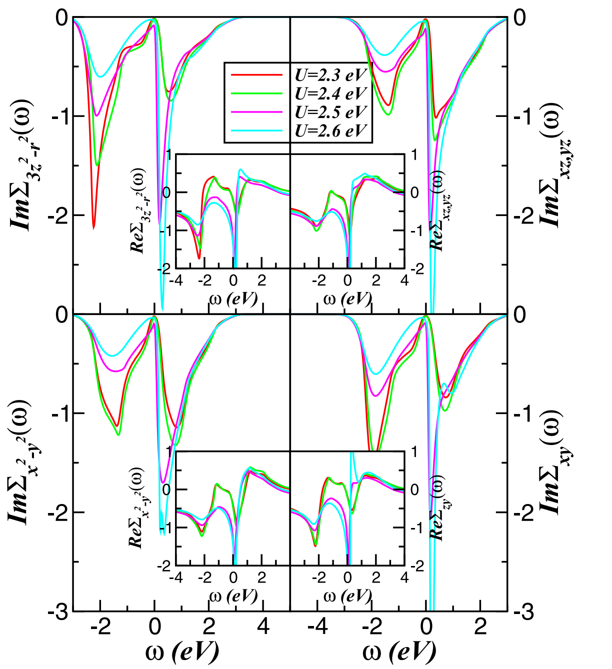

FIG. 6. Orbital-resolved self-energy imaginary (main panels) and real (insets) parts for $3d^8$ $TlNi_2Se_2$, showing their evolution with increasing U for fixed $J_H = 0.7$ eV. Notice the particle-hole asymmetry and the almost perfect Fermi liquid (ω^2) behavior of $\mathrm{Im}\,\Sigma_a(\omega)$ ($a = 3z^2 - r^2, xz, yz, x^2 - y^2$) in metallic $TlNi_2Se_2$. Also interesting is the abrupt change in the ω dependence of $\mathrm{Re}\,\Sigma_a(\omega)$ across the Mott metal-insulator transition.

lead to abrupt modifications of the correlated spectra. Below the critical value of the Mott localized phase ($U_c = 2.5$ eV) the many-body spectra describe a coherent, FL metal with orbital-dependent low-energy Kondo-quasiparticle features. Noteworthy, however, is the suppression of the quasiparticle coherence at low energies at U_c and the emergence of a well-defined V-shaped gap near E_F. Similar Dirac-like electronic dispersion has been reported for $BaFe_2As_2$ [41], suggesting that $3d^8$ $TlNi_2Se_2$ may share a universal band structure with $BaFe_2As_2$ [13], in spite of a chemical potential shift due to there being more $3d$ electrons in $TlNi_2Se_2$ than in $BaFe_2As_2$.

To further characterize the correlated nature of the paramagnetic normal state of $3d^8$ $TlNi_2Se_2$, in Fig. 6 we show the U dependence of the self-energy imaginary (main panels) and real (insets) parts associated with the active Ni-$3d$ orbitals of $TlNi_2Se_2$. Comparing our results with results for the ThFeAsN superconductor [20], for example, we notice similar features despite there being different Coulomb correlation parameters and total electron band fillings n in the two systems, i.e., a clearly visible particle-hole asymmetry in $\Sigma_a(\omega)$, which is intensified with increasing U. This particle-hole asymmetry is also manifested in the self-energy real parts. Interesting as well is the appearance of a peak close to E_F in $\mathrm{Re}\,\Sigma_a(\omega)$ which is strongly enhanced at the Mott transition. Such frequency dependence suggests that Mott localization in the effective $3d^8$ valence state of $TlNi_2Se_2$ is mostly governed by the frequency dependence of the self-energy real parts. While in the orbital-selective metal regime $\mathrm{Im}\,\Sigma_a(\omega)$ shows quadratic frequency dependence, in the Mott-Dirac [42] phase at U_c, $\mathrm{Im}\,\Sigma_a(\omega)$ nearly vanishes at low energies instead of having a pole at E_F, as would occur in a conventional Mott insulator. As pointed out in earlier studies of tetragonal Fe-based materials [20,42], this aspect is somehow reminiscent of marginal, Mott-Dirac liquids where the massive Dirac-like fermions display deviations from the $-\omega^2$ FL form at small ω, which in turn is consistent with (sub)linear ω dependence of marginal FLs [43]. Similar self-energy behavior to that shown in Fig. 6, with sublinear energy dependence, was also found in tetragonal Fe systems [20,42], suggesting hidden marginal Fermi-liquidness at the border of the strain-induced Mott transition in $TlNi_2Se_2$. Finally, since in DMFT the self-energy is momentum independent, the quasiparticle residue Z_a of an orbital a, which defines the renormalized Fermi energy, directly yields the effective electron mass enhancement: $\frac{m_a^\star}{m_e} = \frac{1}{Z_a} = (1 - \frac{\partial\,\mathrm{Re}\,\Sigma_a(\omega)}{\partial\omega})_{\omega=0}$, where m_e is the free electron mass. Thus, from the slope of the self-energy real part we obtain, for $U = 2.4$ eV and $n = 8.0$, $(\frac{m^\star_{3z^2-r^2}}{m_e}, \frac{m^\star_{xz,yz}}{m_e}, \frac{m^\star_{x^2-y^2}}{m_e}, \frac{m^\star_{xy}}{m_e}) = (2.6, 4.0, 3.3, 2.7)$, which is considerably smaller as compared with the heavy-electron effective mass $m^* = (14\text{–}20)m_e$ inferred from electronic specific measurements [4]. It is worth noting that we only observe effective electron mass enhancements consistent with previous observations in the $3d^8$ Mott-Dirac regime. This suggests that there is a complex interplay between MO electronic correlations and electron band filling as the 122-type Ni-based superconductors approach the mixed-valence state [11]. The results presented below illustrate this relationship in more detail.

To rationalize the overall correlated electronic behavior of $TlNi_2Se_2$, in Fig. 7 we compare our orbital-resolved DFT+DMFT result for $U = 2.4$ eV (and $n = 8.0$) with extant energy distribution curves (EDCs) recorded at normal emission for different k directions [9]. As seen, good qualitative agreement between theory and experiment is found over the entire range -1.5 eV $\leqslant \omega \leqslant E_F$. In particular, the energy position of the incoherent one-particle excitation is close to -1.1 eV below E_F, which agrees with the $3z^2 - r^2$ spectral function, as well as the narrow line shape of the Kondo-quasiparticle resonance near E_F. Thus our theory-experiment comparison represents a qualitatively accurate representation of the valence one-electron band structure of $TlNi_2Se_2$ and its link to k (see our results for the angle-resolved photoemission spectroscopy (ARPES) intensity computed along the X-S-Y momentum path using the DFT+DMFT approximation [44] in the inset of Fig. 7) and orbital-resolved spectral functions. Thus, for d^8 $TlNi_2Se_2$, coexisting Kondo-quasiparticle and incoherent components with distinct orbital and k-resolved electronic line shape should be visible at low to moderate binding energies, in spite of large-scale spectral weight transfer induced by sizable electron-electron interactions. Interesting in this context is the crossing point seen at the experimental curves at -0.41 eV, a fingerprint of dynamical transfer of spectral weight. Given the intrinsic $d^{8.5}$ nominal state of $TlNi_2Se_2$, future studies are called for to corroborate our prediction of hidden self-hole-doping behavior possibly due to charge disproportionation of Tl^{2+} to Tl^{1+} and Tl^{3+} [11] in the $TlNi_2Se_2$ superconductor or to valence

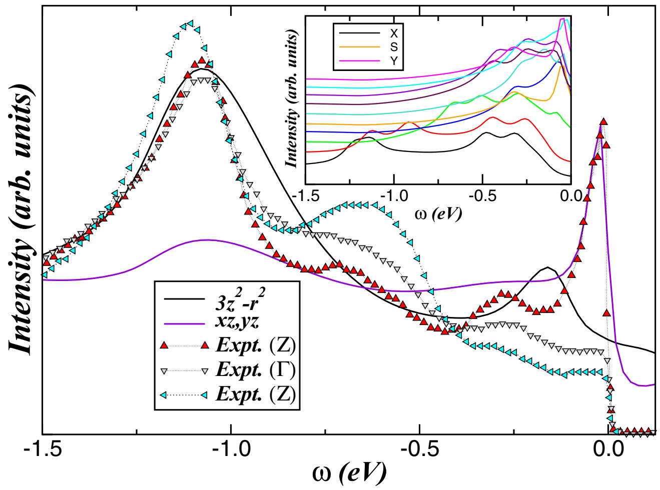

FIG. 7. Theory-experiment comparison between the DFT+DMFT result (for $U = 2.4$ eV, $n = 8.0$) and energy distribution curves (EDCs) taken from Ref. [9]. The theory curve for the xz and yz orbitals is shifted downward in energy by 0.04 eV to coincide with experiment at low energies. Notice the good qualitative theory-experiment agreement at high binding energies, particularly the peak position of the incoherent one-particle excitation close to -1.1 eV below E_F. Also interesting is the nearly similar line shape of the Kondo-quasiparticle resonance in the xz and yz orbitals and the low-energy peak found in experiment in the Z direction as well as the crossing point seen in the experimental curves at -0.41 eV, a fingerprint of dynamical transfer of spectral weight. The inset shows the DFT+DMFT ARPES intensity plot along the X-S-Y momentum path.

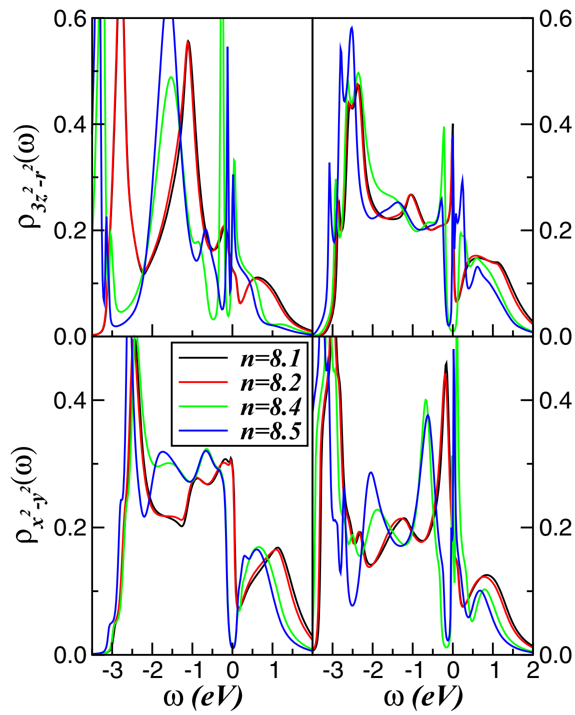

FIG. 8. Effect of increasing the total $3d$ electron occupancy ($n = 8.0 + \delta$) on the orbital-resolved electronic structure of self-hole-doped $TlNi_2Se_2$ computed using $U = 2.4$ eV and $J_H = 0.7$ eV. Particularly interesting features are the robustness of the Fermi liquid metal at small δ and the formation of an orbital-selective electronic state with coexistent insulating $(x^2 - y^2)$, pseudogapped $(3z^2 - r^2)$, and metallic (xz, yz, xy) spectral functions in the mixed-valence ($n = 8.5$) heavy-electron state of $TlNi_2Se_2$.

fluctuating instability similar to that reported for infinite-layer nickelates [45]. Additionally, as discussed for perovskite nickelates [46], the self-hole-doped regime we have found here for $TlNi_2Se_2$ might also come from a hidden charge self-regulation mechanism [47] in which the electronic density around transition-metal cations reorganizes itself in order to preserve the total number of $3d$ electrons (i.e., eight electrons for Ni).

To gain further insight into the normal-state electronic structure reconstruction of $TlNi_2Se_2$, in Fig. 8 we show the effect of increasing the total electron band filling n of the $3d$ shell. This is motivated by the fact that similar to KNi_2Se_2 [8] in an ionic picture the Ni orbital configuration is $3d^{8.5}$ for $TlNi_2Se_2$. Interestingly, this Ni-$3d^{8.5}$ electronic configuration has been proposed [11] to induce the effective band mass enhancement seen in experiment. Therefore understanding the effect of electron band filling is crucial. Despite existing spectroscopy and transport data, the generic appearance of novel states and the instabilities of such states to pseudogap formation [13], and, in particular, to unconventional superconductivity [10], in a wide variety of other correlated electron systems highlight the importance of this question. Our aim here is to build upon the strengths of MO correlated electronic structure modeling to analyze the effect of electron band filling in $TlNi_2Se_2$. In particular, on the basis of explicit calculations, we will present a set of predictions which could be tested in future experiments in the normal state.

In Fig. 8 we show the changes in the correlated electronic structure (for $U = 2.4$ eV and $J_H = 0.7$ eV) upon increasing the total electron concentration ($n = 8.0 + \delta$, with $\delta > 0$) of self-hole-doped $TlNi_2Se_2$. An intriguing observation is that orbital selectivity does not occur at small δ (i.e., $\delta \leqslant 0.2$), showing the robustness of the FL regime to weak electron addition. However, as δ increases to about 0.3, an orbital-selective state develops in stoichiometric $TlNi_2Se_2$. According to our results, orbital selectivity in the $n = 8.5$ mixed-valence state is characterized by the presence of insulating $(x^2 - y^2)$, pseudogapped $(3z^2 - r^2)$, and metallic (xz, yz, xy) spectral functions. The narrow Kondo quasiparticles, responsible for the emergent heavy electrons observed in experiments (see our results in Fig. 8), are particularly intriguing. The origin of these orbital-selective features can be attributed to scattering between different carriers in orbital states split due to specific crystal fields and bare DFT line shape. The latter has two implications: orbital-dependent shifts of the $3d$ bands relative to each other via static Hartree contributions (from the static part of the orbital-dependent self-energies), and strong dynamical correlations due to sizable U, U', and J_H, which cause appreciable spectral weight transfer over large energy scales upon carrier doping. This second feature leads to an orbital-selective modification of the spectral functions, as shown in Fig. 8. Thus, for mixed-valence $TlNi_2Se_2$, coexisting Mott insulating, pseudogapped,

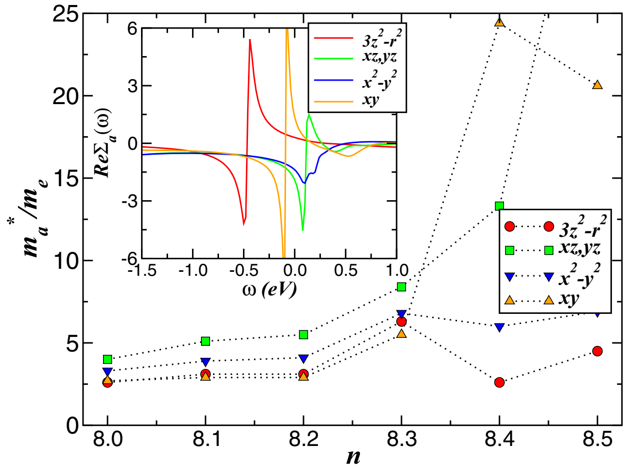

FIG. 9. Evolution of the Ni-3d orbital-resolved effective masses (m_a^*/m_e) with increasing total Ni-band filling ($n = 8 + \delta$) for $U = 2.4$ eV and $J_H = 0.7$ eV, showing strongly enhanced mass renormalization within the $x^2 - y^2$ and $3z^2 - r^2$ orbitals upon electron doping, when approaching the mixed-valence electronic state. The inset shows the orbital-resolved self-energy real parts obtained for $n = 8.4$.

and narrow Kondo components are predicted to emerge at low energies. The hidden orbital selectivity and large-scale dynamical transfer of spectral weight are stringent tests of our proposal for the mixed-valence state, and experimental verification should place it on solid ground.

Lastly, motivated by the emergence of the superconducting state observed in 122-type Ni superconductors from a mixed-valence-driven heavy-electron behavior [11], in Fig. 9 we display the renormalized electron mass as function of total band filling n, computed using the DFT+DMFT orbital-resolved spectral functions of $ThNi_2Se_2$ for $U = 2.4$ eV and $J_H = 0.7$ eV. Our results suggest strong orbital differentiation between the t_{2g} (xy, xz, yz) and e_g $(x^2 - y^2, 3z^2 - r^2)$ orbitals and enhanced mass renormalization within the t_{2g} electronic channel with increasing n. This response is characteristic of strongly correlated materials, where the orbital differentiation is linked to charge and orbital excitations [48] in the reconstructed electronic state at low temperatures. Noteworthy are the effective masses found for $n = 8.4$, which are consistent with $m^* = (14–20)m_e$ [4] and $m^* = (6–18)m_e$ [11] found experimentally, providing support for the orbital-selective mixed-valence heavy-electron state derived within the DFT+DMFT approximation. With these caveats, in the inset of Fig. 9 we show the orbital-resolved self-energy real parts obtained for $U = 2.4$ eV ($J_H = 0.7$ eV) and $n = 8.4$, which could possibly be seen in future experimental studies, similar to a study reported for the correlated normal electronic state of the Sr_2RuO_4 superconductor [49].

III. CONCLUSION

We used a five-orbital Hubbard model treated within the DFT+DMFT framework to investigate the correlation-induced electronic reconstruction in tetragonal $TlNi_2Se_2$. Our results show that the metallic Fermi liquid nature of the compound arises from multiorbital dynamical correlations. Upon electron-doping the self-hole-doped Ni^{2+} valence state, we observe a first-order phase transition from a Fermi liquid metal to an orbital-selective phase with insulating, pseudogapped, and metallic orbitals with narrow Kondo quasiparticles. This transition occurs upon approaching the heavy-electron mixed-valence regime and is accompanied by significant changes in dynamical spectral weight transfer. Our finding of orbital-selective Kondo quasiparticle behavior is relevant to experiments involving heavy electrons with large effective masses which may give rise to multiband superconductivity [4] at low temperatures.

ACKNOWLEDGMENTS

Acknowledgment (L.C.) is given to CNPq and CAPES. S.L. thanks the Leverhulme Trust for support under Project No. RPG-2020-052 as well as ARCCA Cardiff for computational support.

[1] Y. Kamihara, T. Watanabe, M. Hirano, and H. Hosono, Iron-based layered superconductor $La[O_{1-x}F_x]FeAs$ ($x = 0.05–0.12$) with $T_c = 26$ K, J. Am. Chem. Soc. **130**, 3296 (2008); see also F. Ronning, N. Kurita, E. D. Bauer, B. L. Scott, T. Park, T. Klimczuk, R. Movshovich, and J. D. Thompson, The first order phase transition and superconductivity in $BaNi_2As_2$ single crystals, J. Phys.: Condens. Matter **20**, 342203 (2008).

[2] L. de' Medici, G. Giovannetti, and M. Capone, Selective Mott Physics as a Key to Iron Superconductors, Phys. Rev. Lett. **112**, 177001 (2014).

[3] X. Deng, J. Mravlje, R. Žitko, M. Ferrero, G. Kotliar, and A. Georges, How Bad Metals Turn Good: Spectroscopic Signatures of Resilient Quasiparticles, Phys. Rev. Lett. **110**, 086401 (2013).

[4] H. Wang, C. Dong, Q. Mao, R. Khan, X. Zhou, C. Li, B. Chen, J. Yang, Q. Su, and M. Fang, Multiband Superconductivity of Heavy Electrons in a $TlNi_2Se_2$ Single Crystal, Phys. Rev. Lett. **111**, 207001 (2013).

[5] X. C. Hong, Z. Zhang, S. Y. Zhou, J. Pan, Y. Xu, H. Wang, Q. Mao, M. Fang, J. K. Dong, and S. Y. Li, Multigap nodeless superconductivity in nickel chalcogenide $TlNi_2Se_2$, Phys. Rev. B **90**, 060504(R) (2014).

[6] D. C. Johnston, The puzzle of high temperature superconductivity in layered iron pnictides and chalcogenides, Adv. Phys. **59**, 803 (2010); G. R. Stewart, Superconductivity in iron compounds, Rev. Mod. Phys. **83**, 1589 (2011); E. Dagotto, *Colloquium*: The unexpected properties of alkali metal iron selenide superconductors, *ibid.* **85**, 849 (2013).

[7] Z. Li, G. Chen, J. Dong, G. Li, W. Hu, D. Wu, S. Su, P. Zheng, T. Xiang, N. Wang, and J. Luo, Strong-coupling superconductivity in the nickel-based oxypnictide $LaNiAsO_{1-x}F_x$, Phys. Rev. B **78**, 060504(R) (2008).

[8] Q. Fan, X. P. Shen, M. Y. Li, D. W. Shen, W. Li, X. M. Xie, Q. Q. Ge, Z. R. Ye, S. Y. Tan, X. H. Niu, B. P. Xie, and D. L. Feng, Weak electronic correlations and absence of heavy-fermion state in KNi_2Se_2, Phys. Rev. B **91**, 125113 (2015).

[9] N. Xu, C. E. Matt, P. Richard, A. van Roekeghem, S. Biermann, X. Shi, S.-F. Wu, H. W. Liu, D. Chen, T. Qian, N. C. Plumb, M. Radović, H. Wang, Q. Mao, J. Du, M. Fang, J. Mesot, H. Ding, and M. Shi, Camelback-shaped band reconciles heavy-electron behavior with weak electronic Coulomb correlations in superconducting $TlNi_2Se_2$, Phys. Rev. B **92**, 081116(R) (2015).

[10] E. Jellyman, P. Jefferies, S. Pollard, E. M. Forgan, E. Blackburn, E. Campillo, A. T. Holmes, R. Cubitt, J. Gavilano, H. Wang, J. Du, and M. Fang, Unconventional superconductivity in the nickel chalcogenide superconductor $TlNi_2Se_2$, Phys. Rev. B **101**, 134523 (2020).

[11] J. R. Neilson, A. Llobet, A. V. Stier, L. Wu, J. Wen, J. Tao, Y. Zhu, Z. B. Tesanovic, N. P. Armitage, and T. M. McQueen, Mixed-valence-driven heavy-fermion behavior and superconductivity in KNi_2Se_2, Phys. Rev. B **86**, 054512 (2012).

[12] J. R. Neilson, T. M. McQueen, A. Llobet, J. Wen, and M. R. Suchomel, Charge density wave fluctuations, heavy electrons, and superconductivity in KNi_2S_2, Phys. Rev. B **87**, 045124 (2013); see also H. Wang, Q. Mao, H. Chen, Q. Su, C. Dong, R. Khan, J. Yang, B. Chen, and M. Fang, Superconductivity and disorder effect in $TlNi_2Se_{2-x}S_x$ compounds, J. Phys.: Condens. Matter **27**, 395701 (2015).

[13] X. B. Wang, H. P. Wang, H. Wang, M. Fang, and N. L. Wang, Optical properties of $TlNi_2Se_2$: Observation of pseudogap formation, Phys. Rev. B **92**, 245129 (2015).

[14] W. Li, H. Ding, P. Deng, K. Chang, C. Song, K. He, L. Wang, X. Ma, J.-P. Hu, X. Chen, and Q.-K. Xue, Phase separation and magnetic order in K-doped iron selenide superconductor, Nat. Phys. **8**, 126 (2012).

[15] H. Liu, X. Hu, H. Guo, X.-K. Teng, H. Bu, Z. Luo, L. Li, Z. Liu, M. Huo, F. Liang, H. Sun, B. Shen, P. Dai, R. J. Birgeneau, D.-X. Yao, M. Yi, and M. Wang, Single-crystal growth and superconductivity in $RbNi_2Se_2$, Phys. Rev. B **106**, 094511 (2022).

[16] J. Fink, J. Nayak, E. D. L. Rienks, J. Bannies, S. Wurmehl, S. Aswartham, I. Morozov, R. Kappenberger, M. A. ElGhazali, L. Craco, H. Rosner, C. Felser, and B. Büchner, Evidence of hot and cold spots on the Fermi surface of LiFeAs, Phys. Rev. B **99**, 245156 (2019).

[17] Q. Si, Electrons on the verge, Nat. Phys. **5**, 629 (2009); M. M. Qazilbash, J. J. Hamlin, R. E. Baumbach, L. Zhang, D. J. Singh, M. B. Maple, and D. N. Basov, Electronic correlations in the iron pnictides, *ibid.* **5**, 647 (2009).

[18] L. Craco, M. S. Laad, S. Leoni, and H. Rosner, Normal-state correlated electronic structure of iron pnictides from first principles, Phys. Rev. B **78**, 134511 (2008).

[19] L. Craco and S. Leoni, Orbital selectivity in the normal state of KFe_2Se_2 superconductor, Europhys. Lett. **136**, 27002 (2021).

[20] L. Craco and S. Leoni, Orbital-selective nature of the $3d$ electronic structure of the ThFeAsN superconductor, Phys. Rev. B **103**, 075110 (2021).

[21] G. Kotliar, S. Y. Savrasov, K. Haule, V. S. Oudovenko, O. Parcollet, and C. A. Marianetti, Electronic structure calculations with dynamical mean-field theory, Rev. Mod. Phys. **78**, 865 (2006).

[22] G. Prandini, A. Marrazzo, I. E. Castelli, N. Mounet, E. Passaro, and N. Marzari, A Standard solid state pseudopotentials (SSSP) library optimized for precision and efficiency, Materials Cloud Archive **2021.76** (2021).

[23] A. R. Newmark, G. Huan, M. Greenblatt, and M. Croft, Magnetic ordering in $TlCo_{2-x}Ni_xSe_2$ with the $ThCr_2Si_2$ structure, Solid State Commun. **71**, 1025 (1989).

[24] G. Pizzi, V. Vitale, R. Arita, S. Blügel, F. Freimuth, G. Géranton, M. Gibertini, D. Gresch, C. Johnson, T. Koretsune, J. Ibañez-Azpiroz, H. Lee, J.-M. Lihm, D. Marchand, A. Marrazzo, Y. Mokrousov, J. I. Mustafa, Y. Nohara, Y. Nomura, L. Paulatto *et al.*, Wannier90 as a community code: new features and applications, J. Phys.: Condens. Matter **32**, 165902 (2020).

[25] D. Gresch, Q. S. Wu, G. W. Winkler, R. Häuselmann, M. Troyer, and A. A. Soluyanov, Automated construction of symmetrized Wannier-like tight-binding models from *ab initio* calculations, Phys. Rev. Mater. **2**, 103805 (2018); Q. S. Wu, S. N. Zhang, H.-F. Song, M. Troyer, and A. A. Soluyanov, WannierTools: An open-source software package for novel topological materials, Comput. Phys. Commun. **224**, 405 (2018).

[26] F. Lu, J. Z. Zhao, and W.-H. Wang, Electronic structure of the new Ni-based superconductor KNi_2Se_2, J. Phys.: Condens. Matter **24**, 495501 (2012); F. Lu, W.-H. Wang, X. Xie, and F.-C. Zhang, Correlation effects in the electronic structure of the Ni-based superconducting, KNi_2S_2, Phys. Rev. B **87**, 115131 (2013); S. Basak, P. Piekarz, and A. Ptok, Electronic properties and surface states of $RbNi_2Se_2$, Phys. B (Amsterdam) **654**, 414697 (2023).

[27] D. Li, K. Lee, B. Y. Wang, M. Osada, S. Crossley, H. R. Lee, Y. Cui, Y. Hikita, and H. Y. Hwang, Superconductivity in an infinite-layer nickelate, Nature (London) **572**, 624 (2019).

[28] F. Lechermann, Late transition metal oxides with infinite-layer structure: Nickelates versus cuprates, Phys. Rev. B **101**, 081110(R) (2020); Y. Wang, C.-J. Kang, H. Miao, and G. Kotliar, Hund's metal physics: From $SrNiO_2$ to $LaNiO_2$, *ibid.* **102**, 161118(R) (2020); see also H. Chen, A. Hampel, J. Karp, F. Lechermann, and A. J. Millis, Dynamical mean field studies of infinite layer nickelates: Physics results and methodological implications, Front. Phys. **10**, 835942 (2022).

[29] J. Karp, A. Hampel, and A. J. Millis, Dependence of DFT+DMFT results on the construction of the correlated orbitals, Phys. Rev. B **103**, 195101 (2021).

[30] L. Craco and S. Leoni, Orbital-selective mixed-valent Mott/metal phase coexistence in $NdNiO_2$ films, Phys. Rev. Mater. **7**, 044802 (2023).

[31] See L. Craco, M. S. Laad, S. Leoni, and E. Müller-Hartmann, Insulator-metal transition in the doped $3d^1$ transition metal oxide, Phys. Rev. B **70**, 195116 (2004).

[32] See, for example, A. Koga, N. Kawakami, T. M. Rice, and M. Sigrist, Spin, charge, and orbital fluctuations in a multiorbital Mott insulator, Phys. Rev. B **72**, 045128 (2005).

[33] L. Craco, Quantum orbital entanglement: A view from the extended periodic Anderson model, Phys. Rev. B **77**, 125122 (2008).

[34] L. Craco and S. Leoni, Theory of two-fluid metallicity in superconducting FeSe at high pressure, Phys. Rev. B **100**, 121101(R) (2019).

[35] H. Kajueter and G. Kotliar, New Iterative Perturbation Scheme for Lattice Models with Arbitrary Filling, Phys. Rev. Lett. **77**, 131 (1996).

[36] A. Georges, G. Kotliar, W. Krauth, and M. J. Rozenberg, Dynamical mean-field theory of strongly correlated fermion systems and the limit of infinite dimensions, Rev. Mod. Phys. **68**, 13 (1996).

[37] P. Pou, R. Pérez, F. Flores, A. Levy Yeyati, A. Martin-Rodero, J. M. Blanco, F. J. García-Vidal, and J. Ortega, Local-density approach and quasiparticle levels for generalized Hubbard Hamiltonians, Phys. Rev. B **62**, 4309 (2000).

[38] See, for example, N. Dasari, W. R. Mondal, P. Zhang, J. Moreno, M. Jarrell, and N. S. Vidhyadhiraja, A multi-orbital iterated perturbation theory for model Hamiltonians and real material-specific calculations of correlated systems, Eur. Phys. J. B **89**, 202 (2016); see also R. Mizuno, M. Ochi, and K. Kuroki, Development of an efficient impurity solver in dynamical mean field theory for multiband systems: Iterative perturbation theory combined with parquet equations, Phys. Rev. B **104**, 035160 (2021).

[39] L. Craco, Mott-Hubbard and filling-controlled electronic transitions in the layered cuprate oxides, Phys. Rev. B **79**, 085123 (2009).

[40] M. Imada, A. Fujimori, and Y. Tokura, Metal-insulator transitions, Rev. Mod. Phys. **70**, 1039 (1998).

[41] P. Richard, K. Nakayama, T. Sato, M. Neupane, Y.-M. Xu, J. H. Bowen, G. F. Chen, J. L. Luo, N. L. Wang, X. Dai, Z. Fang, H. Ding, and T. Takahashi, Observation of Dirac Cone Electronic Dispersion in $BaFe_2As_2$, Phys. Rev. Lett. **104**, 137001 (2010).

[42] L. Craco and S. Leoni, Selective orbital reconstruction in tetragonal FeS: A density functional dynamical mean-field theory study, Sci. Rep. **7**, 46439 (2017); L. Craco, B. Xu, M. Fang, and B. Freelon, Metal-insulator crossover and massive Dirac fermions in electron-doped FeTe, Phys. Rev. B **101**, 165107 (2020).

[43] C. M. Varma, P. B. Littlewood, S. Schmitt-Rink, E. Abrahams, and A. E. Ruckenstein, Phenomenology of the Normal State of Cu-O High-Temperature Superconductors, Phys. Rev. Lett. **63**, 1996 (1989).

[44] J. Fink, E. D. L. Rienks, S. Thirupathaiah, J. Nayak, A. van Roekeghem, S. Biermann, T. Wolf, P. Adelmann, H. S. Jeevan, P. Gegenwart, S. Wurmehl, C. Felser, and B. Büchner, Experimental evidence for importance of Hund's exchange interaction for incoherence of charge carriers in iron-based superconductors, Phys. Rev. B **95**, 144513 (2017).

[45] A. S. Botana, V. Pardo, W. E. Pickett, and M. R. Norman, Charge ordering in $Ni^{1+}/Ni2+$ nickelates: $La_4Ni_3O_8$ and $La_3Ni_2O_6$, Phys. Rev. B **94**, 081105(R) (2016); Z. Liu, C. Xu, C. Cao, W. Zhu, Z. F. Wang, and J. Yang, *ibid.* **103**, 045103 (2021); K. G. Slobodchikov and I. V. Leonov, Spin density wave, charge density wave, and bond disproportionation wave instabilities in hole-doped infinite-layer RNiO$_2$, *ibid.* **106**, 165110 (2022).

[46] L. Iglesias, M. Bibes, and J. Varignon, First-principles study of electron and hole doping effects in perovskite nickelates, Phys. Rev. B **104**, 035123 (2021).

[47] H. Raebiger, S. Lany, and A. Zunger, Charge self-regulation upon changing the oxidation state of transition metals in insulators, Nature (London) **453**, 763 (2008).

[48] See, for example, N. D. Patel, A. Nocera, G. Alvarez, A. Moreo, S. Johnston, and E. Dagotto, Fingerprints of an orbital-selective Mott phase in the block magnetic state of $BaFe_2Se_3$ ladders, Commun. Phys. **2**, 64 (2019).

[49] A. Tamai, M. Zingl, E. Rozbicki, E. Cappelli, S. Riccò, A. de la Torre, S. McKeown Walker, F. Y. Bruno, P. D. C. King, W. Meevasana, M. Shi, M. Radović, N. C. Plumb, A. S. Gibbs, A. P. Mackenzie, C. Berthod, H. U. R. Strand, M. Kim, A. Georges, and F. Baumberger, High-Resolution Photoemission on Sr_2RuO_4 Reveals Correlation-Enhanced Effective Spin-Orbit Coupling and Dominantly Local Self-Energies, Phys. Rev. X **9**, 021048 (2019).